Journal of CO_2 Utilization 25 (2018) 68–78

Contents lists available at ScienceDirect

Journal of CO_2 Utilization

journal homepage: www.elsevier.com/locate/jcou

Multicomponent Ni-CeO_2 nanocatalysts for syngas production from CO_2/CH_4 mixtures

E. le Saché[a], J.L Santos[b], T.J. Smith[a], M.A. Centeno[b], H. Arellano-Garcia[a], J.A. Odriozola[b], T.R. Reina[a,*]

[a] Department of Chemical and Process Engineering, Faculty of Engineering and Physical Sciences, University of Surrey, Guildford, UK
[b] Departamento de Química Inorgánica e Instituto de Ciencias de Materiales de Sevilla. Centro mixto US-CSIC Avda. Américo Vespucio 49, 41092 Seville, Spain

ARTICLE INFO

Keywords:
Syngas production
CO2 utilisation
Ni catalysts
Cerium oxide
Bimetallic catalysts

ABSTRACT

The dry reforming of methane with CO_2 is a common route to transform CO_2/CH_4 mixtures into added value syngas. Ni based catalysts are highly active for this goal but suffer from deactivation, as such promoters need to be introduced to counteract this, and improve performance. In this study, mono- and bi-metallic formulations based on 10 wt.% Ni/CeO_2-Al_2O_3 are explored and compared to a reference 10 wt.% Ni/γ-Al_2O_3. The effect of Sn and Pt as promoters of Ni/CeO_2-Al_2O_3 was also investigated. The formulation promoted with Sn looked especially promising, showing CO_2 conversions stabilising at 65% after highs of 95%. Its increased performance is attributed to the additional dispersion Sn promotion causes. Changes in the reaction conditions (space velocity and temperature) cement this idea, with the Ni-Sn/CeAl material performing superiorly to the mono-metallic material, showing less deactivation. However, in the long run it is noted that the mono-metallic Ni/CeAl performs better. As such the application is key when deciding which catalyst to employ in the dry reforming process.

1. Introduction

Carbon dioxide is one of the major issues facing the world currently, the adverse effects on the environment that CO_2 emissions cause are well documented and are causing global concern; with the year 2014 seeing 35.7 billion tonnes of CO_2 produced from fossil fuel combustion and industrial processes alone [1]. However, industry is taking major steps to help mitigate these effects, by capturing a proportion of the CO_2 being produced each year. The array of technology used to capture CO_2 is large, including absorption in liquids [2] and adsorption on solids [3], which can be implemented either pre- or post-combustion depending on the application. The scheme to reduce atmospheric carbon emissions via capture is part of a worldwide initiative, with the captured carbon being stored by geological, mineralisation or oceanic means. Nevertheless, a lot of progress needs to be made within this field before it becomes a truly viable option [4,5].

An alternative solution can be employed instead of storage, namely the chemical upgrading of CO_2 to fuels and chemicals. In addition to the depletion of CO_2 emissions, extra motivation is provided by the generation of value-added products [6].

Among the different alternatives for CO_2 utilisation, the dry reforming of methane (DRM, Eq. (1)) is a promising route and has the added benefit of utilising methane which has a global warming potential 25 times that of CO_2 [7]:

$$CH_4 + CO_2 \rightleftharpoons 2CO + 2H_2 \quad (1)$$

$$\Delta H_{298K} = +247\,kJ/mol$$

$$\Delta G_{298K} = +170\,kJ/mol$$

This route leads to the production of syngas (H_2 and CO) [8], which is a highly useful and valuable intermediary. It can be used as a precursor in chemical processes, such as methanol production and the Fischer-Tropsch Synthesis (FTS) to create long chain hydrocarbons (e.g. diesel) [9].

Besides natural gas, there are several different sources of methane that can be utilised to coincide with the theme of fossil fuel and emissions awareness. For instance, biogas produced by the anaerobic digestion of organic matter is also the dominant mechanism for producing landfill gas; the main constituent of which is biogas. Both have roughly equal concentrations of methane and carbon dioxide [8].

However, the dry reforming operational conditions impose some challenges to develop this technology. For instance, due to the endothermic nature of the reaction and the high stability of the reactants (methane and carbon dioxide), high temperatures and suitable catalysts are needed to achieve optimal conversions and selectivity to syngas. Unfortunately, high temperatures also cause catalyst deactivation. This

* Corresponding author.
E-mail address: t.ramirezreina@surrey.ac.uk (T.R. Reina).

https://doi.org/10.1016/j.jcou.2018.03.012
Received 28 November 2017; Received in revised form 13 February 2018; Accepted 12 March 2018
Available online 20 March 2018

can be via sintering of the active metal phase, or by the promotion of side reactions forming solid carbon [8,10]. This carbon then deposits on the catalyst, blocking the active phase [11]. This deposition can proceed by the Boudouard reaction (BR, Eq. (2)), methane decomposition (Eq. (3)) and CO reduction (Eq. (4)):

$$2CO \rightleftharpoons C(s) + CO_2 \quad (2)$$

$$CH_4 \rightleftharpoons C(s) + 2H_2 \quad (3)$$

$$CO + H_2 \rightleftharpoons C(s) + H_2O \quad (4)$$

Methane decomposition especially is known to occur on Ni particles. Carbon remains adsorbed on the metal particles preventing access to the active metallic phase and thus decreasing the catalytic performance [12]. Carbon formation is favored by larger Nickel particles, therefore when sintering occurs during the reaction it enhances carbon deposition. Thus sintering has a double effect on the catalyst activity: first the active surface decreases altering the catalytic activity and second carbon formation is more favored on bigger particles leading to a faster deactivation of the catalyst [8,11].

Hence an effective dry reforming catalyst must be resistant to sintering as well the formation of (hard) carbon upon its surface. Concurrently, it must be relatively inexpensive and produce optimal conversions, such that it can realistically be employed in medium and large-scale applications.

Traditionally, Ni based materials are the state of the art catalysts for reforming reactions, [8,13–16,12] and for the dry reforming in particular [8,10,17]. Nevertheless, Ni is highly prone to nucleate carbonaceous deposits and to undergo sintering, resulting in severe activity depletion [17–19]. In response to these drawbacks a great deal of work in the last decade have been focused on the application of precious metal based catalysts, for reforming reactions [20]. Catalysts based on Rh [21–23], Ru [24,25] Pt [20,26,27] among others systems can outperform Ni and overcome partially or completely the stability issues. However, their cost makes them unviable for a realistic application.

Alternatively, Ni based materials can be promoted, reducing the impact of sintering and coking and improving the overall performance. Recently, Pastor-Perez et al demonstrated that a multicomponent catalyst based on Ni-CeO_2 is a good choice for glycerol reforming [28]. The introduction of CeO_2 in the catalysts formulation reduces the acidity and increases the oxygen mobility of the support [27,29], both factors helping to avoid carbon deposition. In addition, bimetallic combinations i.e. Ni-Fe, Ni-Co, Ni-Sn [19,30], Ni-Pt [20,26,31,32] have been studied, showing in some cases very promising results. In particular, Ni-Sn materials have proven to be of interest towards reforming reactions [30,33,34]. Similarly to carbon, tin contains p electrons in its outer shell close to a stable s-orbital. When carbon is present the 3d electrons of nickel interact with the 2p electrons of carbon to form nickel carbide. The presence of tin would favours the interaction of Sn p orbitals with Ni 3d electrons, thereby reducing the chance of nickel carbide formation as a coke precursor [12]. However, in large amounts tin inhibits reactant conversions. Hou et. al. studied the effect of tin addition on coke formation and the catalytic activity of Ni/α-Al_2O_3 for DRM and found that a Sn/Ni molar ratio of 0.02 was the optimum trade-off between the loss of activity and the prevention of coke formation [19]. On the other hand, the promotion of Ni catalysts with low amounts of noble metal is also of interest: a low cost Ni catalyst would benefit from the C-resistance and enhanced activity of a noble metal. Ni-Pt catalysts showed promising results with Pt loadings as low as 0.3 wt% [20,26]. The introduction of Pt was found to ease the reduction of NiO, to better disperse Ni particles and help achieving smaller Ni particles [20,32,31].

In summary, the promoter can be included in the metallic phase, in the support or in both, leading to multicomponent materials with enhanced catalytic features.

Under these premises, the aim of this work is to develop advanced multicomponent catalysts for chemical CO_2 recycling via the dry reforming of methane. Following a sequential design strategy (going from the simplest Ni/Al_2O_3 to the most complex design Ni-Sn/CeO_2/Al_2O_3 or Ni-Pt/CeO_2/Al_2O_3) we have developed highly efficient materials for dry reforming, while revealing the key aspects for a successful catalyst design.

2. Experimental

2.1. Catalyst preparation

The Cerium promoted support was synthesized by impregnation of $Ce(NO_3)_2{\cdot}6H_2O$ (Sigma-Aldrich) on γ-Al_2O_3 (Sasol –SCFa-230) in order to obtain a 20 wt% loading of CeO_2. This support, named "CeAl" was calcined at 800 °C for 8 h. The different active phases were added by sequential wet impregnation starting with the impregnation of Ni using $Ni(NO_3)_2{\cdot}6H_2O$ (Sigma-Aldrich) and a calcination step of 800 °C for 4 h. The second impregnation involved either $H_2Cl_6Pt{\cdot}6H_2O$ (37.5%, Sigma-Aldrich) or $SnCl_2{\cdot}2H_2O$ (Sigma-Aldrich) and calcination at 800 °C for 4 hours. The metal loading of the catalysts was calculated to be 10 wt.% of Ni, 0.3 wt.% of Pt and 0.4 wt.% of Sn (molar Sn/Ni = 0.02). For sake of simplicity, oxygen is omitted in the selected nomenclature. The prepared catalysts are then called Ni/Al, Ni/CeAl, Ni-Sn/CeAl and Ni-Pt/CeAl.

2.2. Catalyst characterisation

X-ray diffraction (XRD) patterns were recorded on an X'Pert Pro PANalytical, using Cu Kα radiation (40 mA, 45 kV). The spectra were registered over a 2θ range between 10–90 °, with an angle increase of 0.05° every 160 s.

Temperature programmed reduction with hydrogen (H_2-TPR) analysis was carried out on the calcined catalyst in a U-shaped quartz reactor. A gas flow of 50 ml min^{-1} of 5% H_2 in an Ar atmosphere (Air Liquide) was utilised. A 50 mg catalyst sample was heated at a rate of 10 °C min^{-1} from room temperature to 900 °C. Utilising an on stream thermal conductivity detector (TCD) to monitor the hydrogen consumption.

The textural properties of the catalyst were analysed by N_2 adsorption-desorption experiments at −196 °C (liquid nitrogen temperature). The measurements were performed on a Micromeritics Tristar 22. With the samples being degassed for 2 h at 250 °C in vacuum, before the analysis.

Raman spectroscopy was performed on the used catalytic samples. With the measurements being taken on a Horiba Jobin Yvon dispersive microscope (HR800) with confocal aperture 1000 µm, using a laser spot diameter of 0.72 µm and spatial resolution of 360 nm. The microscope was equipped with a diffraction grating of 600 grooves/mm, and a CCD detector, using a green laser (λ = 532.14 nm, maximum power 20 mW) and a 100 × objective.

Scanning electron microscopy (SEM) analysis was performed on both the fresh and used samples in a vacuum. Utilising a JEOL 5400 microscope equipped with an EDS analyser (Oxford Link).

The temperature-programmed oxidation (TPO) was carried out in a U-shaped reactor under a total flow of 50 mL min^{-1} (5% O_2 in He) from room temperature to 900 °C with a heating rate of 10 °C min^{-1}. The formed products were analysed by mass spectrometry (MS) in a Pfeiffer vacuum mass spectrometer.

2.3. Catalytic tests

The catalytic behaviour of the prepared samples for the dry reforming of methane was carried out under atmospheric pressure in a continuous flow quartz tube reactor. The reactor set up is detailed in Fig. 1. For each catalyst screening reaction, 0.1 g (particle size 100–200 µm) of catalyst was supported upon a reactor bed of quartz wool. The catalyst was reduced in situ in a 100 mL/min flow containing

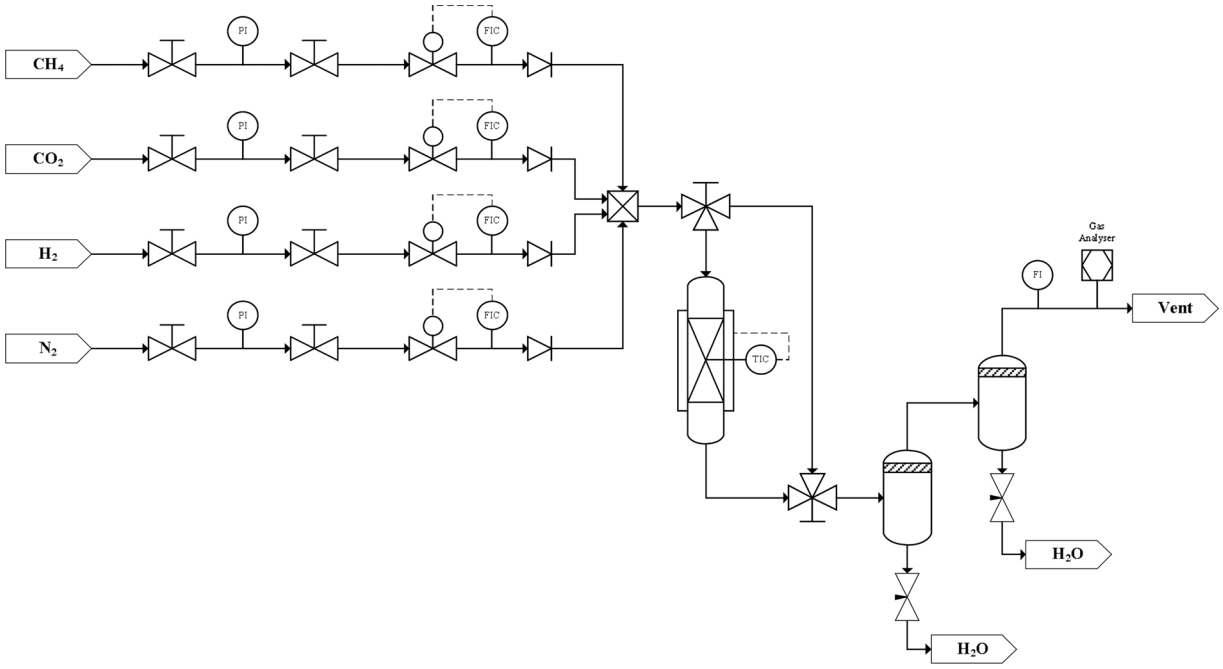

Fig. 1. Process flow diagram (PFD) for experimental set up.

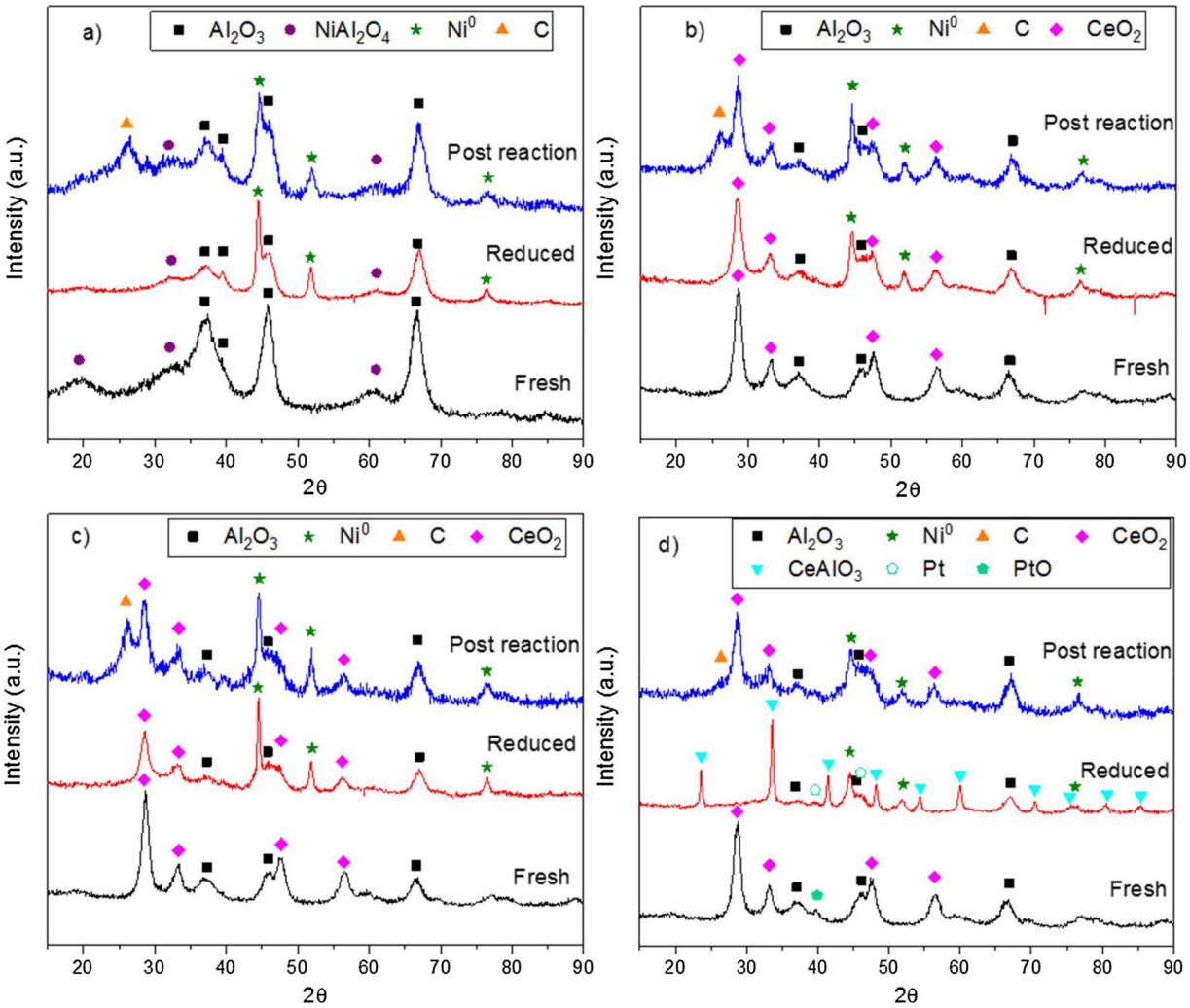

Fig. 2. XRD characterisation spectra for sample catalyst: (a) Ni/Al, (b) Ni/CeAl, (c) Ni-Sn/CeAl and (d) Ni-Pt/CeAl, calcined, reduced and post reaction.

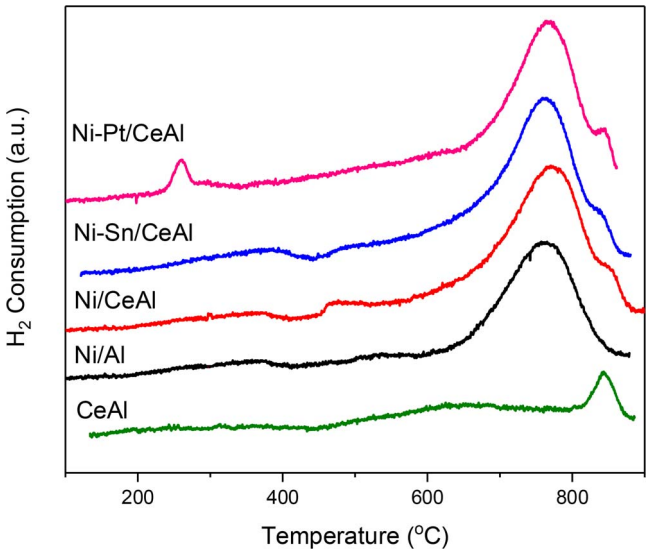

Fig. 3. H_2-TPR profiles for the sample catalysts and support.

Table 1
Textural properties of the prepared samples.

Catalyst	S_{BET} ($m^2\ g^{-1}$)	Pore Volume ($cm^3\ g^{-1}$)
Ni/Al	164	0.42
Ni/CeAl	116	0.28
Ni-Sn/CeAl	120	0.29
Ni-Pt/CeAl	118	0.28

20% H_2 in N_2 at 800 °C for 1 h with a heating rate of 15 °C/min. Reactions were conducted in a 100 mL/min flow containing 12.5% CH_4, 12.5% CO_2 and 75% N_2 (WHSV = 60,000 mL g^{-1} h^{-1}), at temperature values ranging from 600 °C to 800 °C. For the reactions where the space velocity is varied, this is achieved by increasing or decreasing the mass of the catalyst sample used (0.05 g: 120,000 mL g^{-1} h^{-1}; 0.2 g: 30,000 mL g^{-1} h^{-1}). A stability test was conducted at 700 °C with a WHSV of 60,000 mL g^{-1} h^{-1} for about 100 h.

In all the experiments, the composition of the gas product stream leaving the reactor was analysed by an on-stream gas analyser (ABB AO2020). The spent samples were recovered for post reaction characterisation.

The conversions of the reactants as well as the H_2/CO ratio were used to evaluate the catalytic performance of each sample. The following equations were used to determine these conversions [10].

$$X_{CH_4}(\%) = \frac{F_{CH_4,in} - F_{CH_4,out}}{F_{CH_4,in}} \times 100$$

$$X_{CO_2}(\%) = \frac{F_{CO_2,in} - F_{CO_2,out}}{F_{CO_2,in}} \times 100$$

3. Results and discussion

3.1. X-Ray diffraction (XRD)

Fig. 2 shows the XRD patterns for all the sample catalysts. For the fresh catalyst samples, there are no characteristic crystalline peaks that can be attributed to metallic or oxidised Ni species. This indicates that the Ni is highly dispersed and has a small particle size. Nevertheless, the presence of nickel aluminate spinels ($NiAl_2O_4$) cannot be discarded, but the spinel crystalline peaks overlap with the (4 4 0), (4 0 0) and (3 1 1) planes, of the gamma phase of alumina at 66.79°, 45.76° and 37.58° respectively. Indeed, as previously reported elsewhere, the Ni loading is critical to fully form spinels [35]. In our case, 10 wt.% Ni is not enough to transform all the γ-Al_2O_3 into $NiAl_2O_4$, in which the Ni content is around 33 wt.%. Therefore, surface $NiAl_2O_4$ spinels should co-exists with the γ-Al_2O_3 support (JCPDS 00-004-0880) [35].

As for the ceria containing samples (Fig. 2b–d), all the catalysts show the diffractions peaks for ceria fluorite type structures, at a 2θ of 28°, 33°, 48° and 56° (JCPDS# 00-004-0593). Ni-Sn/CeAl (Fig. 2c) shows a very similar pattern to that exhibited by the monometallic Ni/CeAl (Fig. 2b). No evidence of Ni-Sn alloys are detected in the fresh material, in good agreement with previous results for similar catalysts [28]. The XRD pattern of Ni-Pt/CeAl (Fig. 2d) shows a pattern comparable to that depicted for Ni/CeAl (Fig. 2b), with the exception of a small at 2θ = 39° attributed to PtO (JCPDS 43-1100).

As prior to the reaction the samples are activated in hydrogen, it is relevant to study the changes taking place during this treatment. In fact, very useful information is obtained from the XRD patterns of the reduced samples (Fig. 2a–d). For all the catalysts a new phase corresponding to metallic Ni nanoparticles (JCPDS 87-0712) was detected indicating that metallic Ni will be the predominant active phase for the reaction. Interestingly, the fluorite structure collapses for the Pt-Ni bimetallic sample and leads to the formation of cerium aluminate. The later agrees with the observation of Prakash and co-workers who identified the formation of this phase when ceria on γ-alumina is reduced using a hydrogen atmosphere [36]. The presence of platinum favours this reduction which does not happen for the Ni-Sn/CeAl and the Ni/CeAl catalysts. Indeed, Pt on CeO_2/Al_2O_3 assists the reversible formation of $CeAlO_3$ upon reduction under H_2 and high temperature (here 800 °C) [37]. After reaction the Ni-Pt catalyst recovers the ceria phase (Fig. 2d) under oxidising conditions in good agreement with literature [37]. Also for this sample the Ni particle size (estimated using Scherrer equation) is the smallest within the studied series (i.e ~12 nm before and after the reaction while for the rest of the materials the Ni particle size is around 20–25 nm in all the cases for fresh and spent samples). Indeed, the addition of Pt was found to improve metal dispersion and to reduce Ni particle size in previous studies [32,31]. The spent samples also present a peak ascribed to filamentous carbon at 2θ = 26°, corroborating the formation of surface carbon during the reforming reaction. Here again, the Pt based materials behaves differently showing no evidence of carbon formation in the XRD pattern which suggests that the carbon formed on Ni-Pt/CeAl is mostly amorphous in its structure.

3.2. H_2-Temperature programmed reduction (H_2-TPR)

The temperature programmed reduction was undertaken so interactions between the support and metallic species, as well as the redox properties of the catalysts can be assessed.

H_2-TPR profiles are shown in Fig. 3, the profile obtained for Ni/Al contains a major peak at a high temperature of 650–850 °C, which is ascribed to the reduction of $NiAl_2O_4$ spinels [27,38]. These species require high temperatures to be reduced due to the close packed structure, agreeing with the XRD data [39]. The CeAl support only contains a small peak at 850 °C corresponding to the reduction of bulk ceria crystallites [40]. The profiles pertaining to Ni/CeAl, Ni-Sn/CeAl and Ni-Pt/CeAl contain the major peak attributed to the reduction of $NiAl_2O_4$ spinels [41] in addition to a marked elbow in the 850 °C region attributed to the reduction of CeO_2. The Ni-Pt/CeAl profile exhibit an extra small peak representing the reduction of PtO species at a temperature of 250 °C [37,42]. Overall, the prepared catalysts present certain degree of oxygen mobility in the reaction temperature range 600–850 °C which may influence their observed performance.

3.3. Textural properties

The textual properties for the prepared sample catalysts are presented in Table 1, showing specific surface area (S_{BET}) and the average

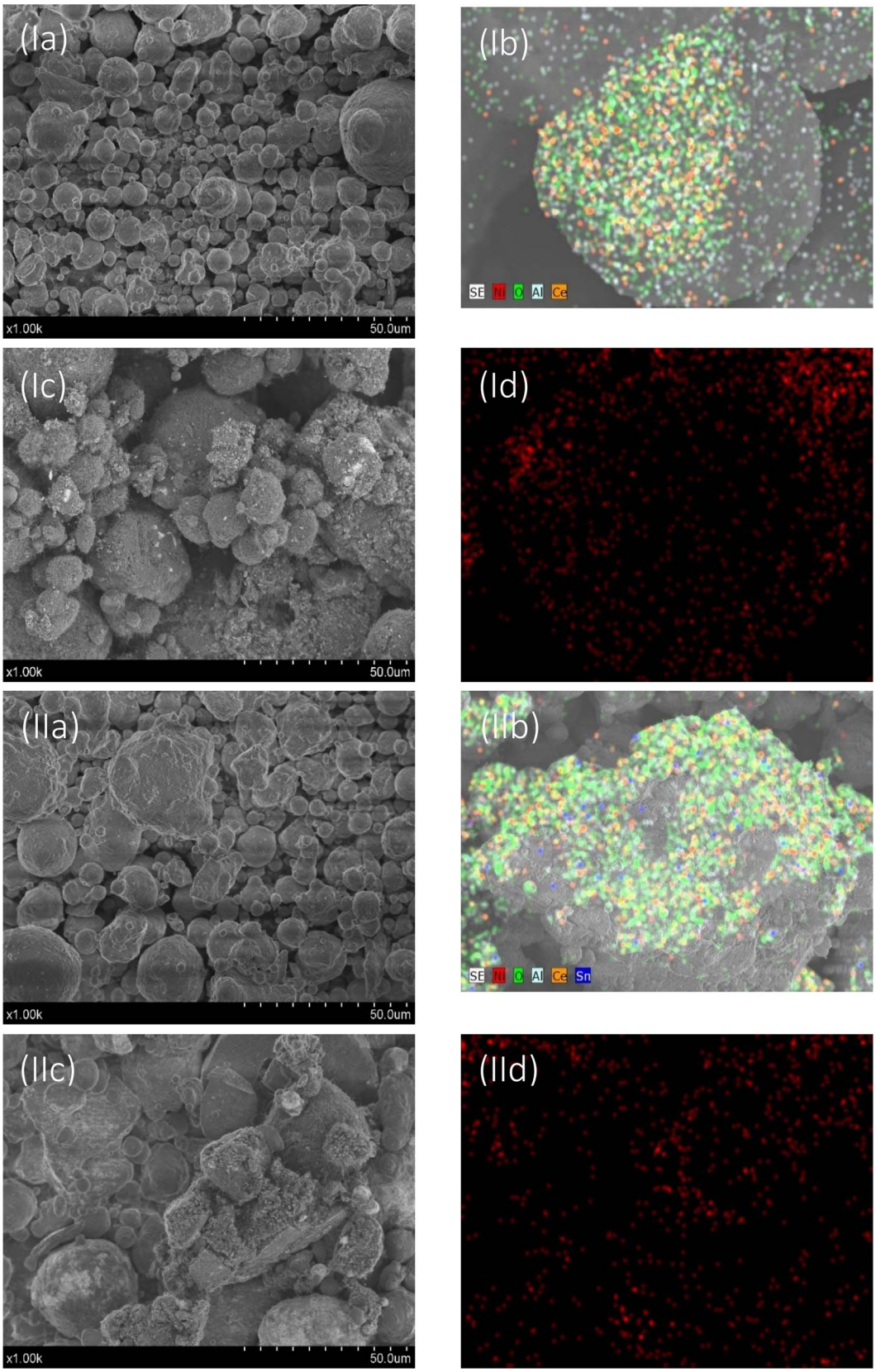

Fig. 4. SEM images of catalysts: (I) Ni/CeAl and (II) Ni-Sn/CeAl (for all samples: (a) fresh catalyst, (b) general mapping of fresh catalyst, (c) used catalyst, (d) carbon mapping of used catalyst.

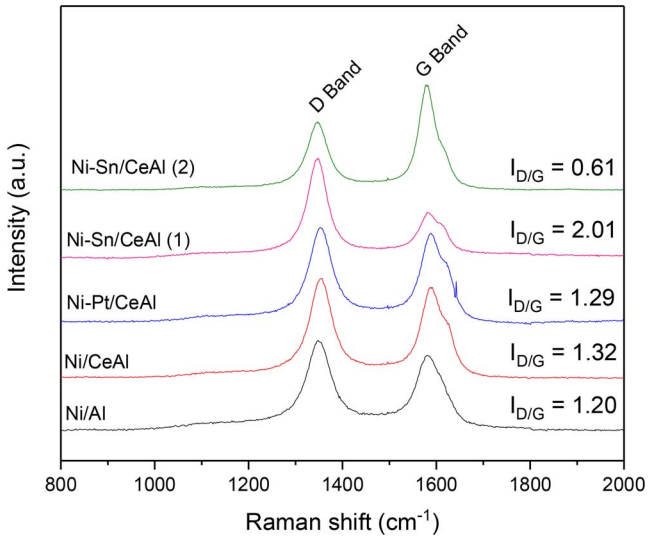

Fig. 5. Raman spectra of the used catalysts where Ni-Sn/CeAl (1) and Ni-Sn/Ce-Al (2) refer to two different zones of the same Ni-Sn/CeAl sample.

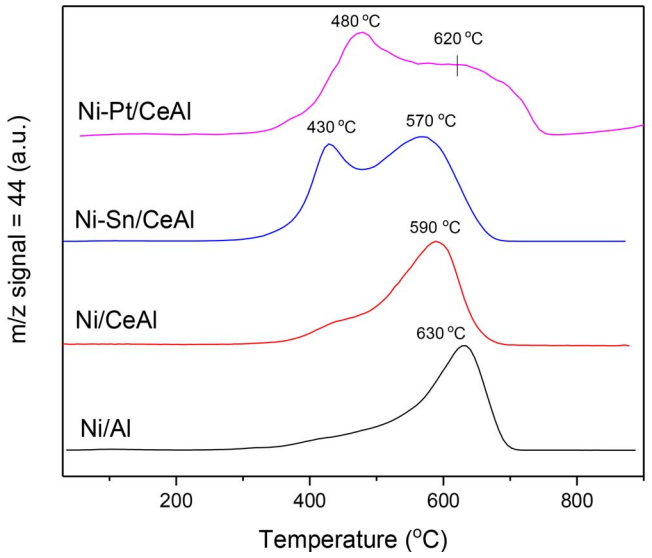

Fig. 6. TPO profiles of the used catalysts.

volume of the pores for each catalyst.

The N_2 adsorption-desorption isotherms for all the catalyst samples (not shown) correspond to type IV isotherms, indicating multilayer adsorption as well as being characteristic of a material containing mesopores. The specific surface area of the catalyst samples drops with the addition of ceria (Table 1). This effect has been previously reported [43] and has been attributed to ceria species covering the surface area of the Al_2O_3. This is corroborated by a corresponding decrease in the volume of the mesopores, which also partly explains the lower specific surface area when compared to γ- Al_2O_3.

By comparison, the addition of the promoters Sn and Pt does not influence the textural properties of the catalysts. This could be due to the relatively small quantities of the promoters utilised. As such, they are highly dispersed, resulting in little to no effect despite being intrinsically less porous [44].

3.4. SEM

Fig. 4 shows the SEM images used in the examination of the morphology and texture of the catalysts. From the fresh images (Fig. 4a), it can be deduced that the morphology of the samples are comparable to one another, with micro-, nano-and larger particles all present. These larger particles can be assumed to be Al_2O_3, whilst some of the nano- and micro- particles can be Ni° and/or NiO and CeO_2. This is supported by the general EDS-mapping of the catalyst (Fig. 4b), which shows the distribution of Ni, Al, Ce and O.

Examination of the catalyst samples post reaction (Fig. 4c) shows a major transformation in catalyst morphology. This is down to the presence of filamentous carbon deposits, on the samples' surface. The presence of similar quantities of crystalline structures are noted on both catalyst samples, attributed to graphitic carbon [45]. The distribution of carbonaceous species is visualised by carbon mapping in Fig. 4d. Both samples show an even distribution of carbon which agrees with the Ni particles dispersion since Ni atoms are the main carbon nucleation site during the reaction.

3.5. Raman

Raman spectroscopy was used to characterize the structure of the carbon deposited onto the spent catalyst samples, Fig. 5. Two characteristic peaks typically ascribed to sp^2 bonded carbon species are present [30]. The peak at 1350 cm^{-1} called D-band is indicative of carbon atoms in a disordered amorphous carbon network [46]. The peak at 1585 cm^{-1} on the other hand corresponds to the G-band, associated with graphitic carbon due to a high degree of order, symmetry and crystallinity [47,48]. The shape, position and relative intensities of these bands vary slightly over the studied series of samples, indicating some structural differences in the type of carbon formed over the investigated catalysts. The key Raman parameter to monitor carbon bonding is the intensity ratio of the *D* and *G* peaks, I_D/I_G. In amorphous carbons I_D/I_G is a measure of the size of the sp^2 phase organized in rings. I_D/I_G which indicates the degree of crystallinity of the carbon varies across the series as shown in the Fig. 5 inset. In fact, this ratio reflects the impact of the promoters in the carbon formation, with the Ni/Al sample showing the lowest value and therefore the most graphitic carbon. The presence of CeO_2 alleviates the graphitisation degree resulting in higher I_D/I_G ratios. Although in every sample several carbon Raman spectra with different I_D/I_G can be obtained, the situation is more evident in the Ni-Sn one, where two types or carbon were detected with a marked disparity in terms of crystalline degree. Two extreme situations were witnessed in the Ni-Sn sample I_D/I_G = 2.01 corresponding to a soft carbon with amorphous character and I_D/I_G = 0.61 ascribed to well-structured hard carbon. In any case it is clear that the presence of promoters such as CeO_2 and the bimetallic formulations Ni-Sn or Ni-Pt influences the mechanisms of carbon formation as well as the tolerance of the catalysts towards coking [49,50].

However, the Raman data needs further support to extract conclusive indications of the carbon deposition over the multicomponent catalysts. In this sense, TPO analysis of the spent samples were conducted and they are presented in Fig. 6.

3.6. TPO

TPO experiments of the spent catalysts after 20 h of reaction were performed to investigate the nature of the carbonaceous species deposited on the surface of the catalysts. The evolution of CO_2 signal (m/z = 44) was analysed by MS and the results are shown in Fig. 6. The temperature at which a maximum of CO_2 production is observed gives information on the type of the carbonaceous species deposited on the surface. The Ni/Al and Ni/CeAl profiles show a peak at around 600 °C which has been attributed to highly structured carbon being present, as it requires high temperatures to be oxidised. A careful analysis of the profiles indicates another oxidation process at lower temperatures 400-500 °C which denotes the presence of softer carbon in lower proportion. The presence of two type of carbons is clearly evident for the bimetallic catalysts. The plot for Ni-Sn/CeAl shows two peaks at 430 and 570 °C while the profile Ni-Pt/CeAl reveals two oxidation processes at about

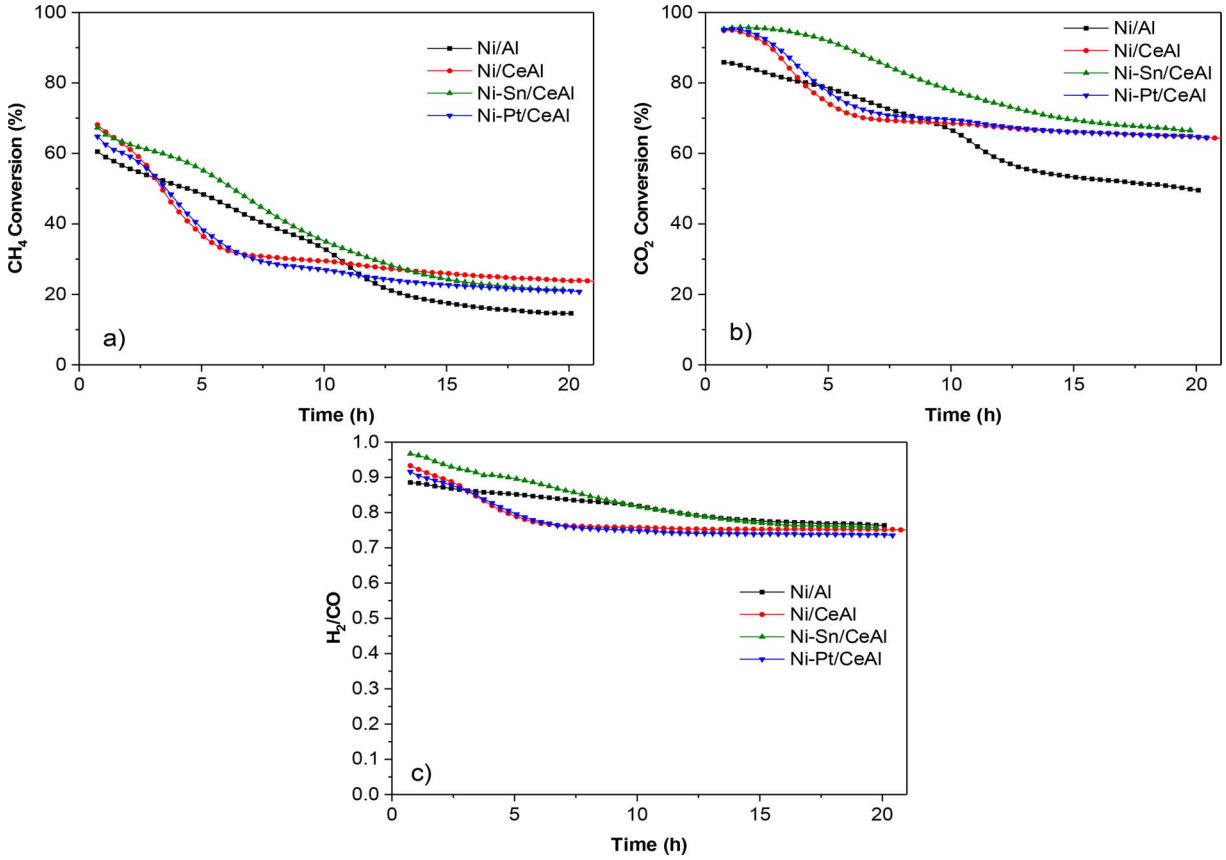

Fig. 7. Catalyst screening: a) CH_4 conversions (%), b) CO_2 conversions (%) and c) H_2/CO ratio (Reaction conditions: WHSV = 60,000 ml g^{-1} h^{-1}; CH_4:CO_2 = 1; P = 1 atm, T = 700 °C).

480 and 620 °C. These observations match perfectly with the presence of multiple types of carbon in good agreement with the Raman analysis. In the case of the Ni-Sn system, both peaks appear at lower temperatures compared to those of the Ni/Al and Ni/CeAl indicating that softer forms of carbon having been formed by using the bimetallic combination [32,46].

3.7. Catalytic behaviour

The catalytic behaviour of the prepared catalysts in terms of CH_4 and CO_2 conversions, as well as H_2/CO ratio is shown in Fig. 7, as a function of time on stream. It can clearly be seen that as time on stream progresses, the conversion of both CH_4 and CO_2 decrease for all catalysts. This drop in activity indicates the formation of inactive carbon on the surface of the catalyst (as shown by the SEM images, Fig. 4d and XRD patterns). It must be noticed though that all the promoted catalysts perform much better that the reference Ni/Al sample which showed the poorest activity, reaching a steady state conversion of 18% for CH_4 and 48% for CO_2. In contrast, the Ni/CeAl catalyst stabilises at superior conversions, namely around 25% for CH_4 and around 65% for CO_2 conversion. The impact of ceria is therefore evident in the catalytic performance. Several reasons may account for the beneficial effect of ceria. Firstly, it reduces the overall acidity of the bare support (alumina), which helps to avoid carbon nucleation given the direct correlation between acid sites and coking [23,51]. Secondly, the excellent redox properties of ceria (i.e. its large oxygen storage capacity – OSC) help to mitigate carbon deposition, by facilitating the oxidation and/or gasification of the carbonaceous species nucleating on the surface during dry reforming [29,43,49]. The greater activity of ceria based samples is therefore directly correlated with the above mentioned capacity of ceria to mitigate coking which is in fair agreement with the TPR data discussed above and the TPO profiles of the spent samples described in Fig. 6.

The effects on the conversions caused by the addition of promoters to the Ni/CeAl catalyst differ. The Sn promoted catalyst exhibited a marked increase in both CO_2 and CH_4 conversions to begin with, before a drop in catalytic activity and reaching stable conversions similar to those of Ni/CeAl base catalyst. In any case, this catalyst seems to be the best one with a remarkable advantage in the early reaction stages. By contrast, promotion of Ni/CeAl by Pt appears to hardly affect the activity of the catalyst at all, with no remarkable change in the conversion values. Despite some authors report in literature that tiny amounts of Pt can be enough to boost the performance of Ni based catalysts [20], our results indicate that in the dry reforming of methane, a Pt loading below 0.3 wt. % does not influence the performance. The H_2/CO ratio for all the catalysts were very similar, with a final value after 20 + hours on stream in the region of 0.75–0.8, very close to 1 which is the limit imposed by the nature of the reaction. Very interestingly, the Sn promoted catalyst shows the highest initial ratio of 0.97, which is probably related to the higher level of conversion reached by this sample at the beginning of the catalytic run.

From the catalytic screening, it can be concluded that Sn is a promising promoter. In order to assess whether it is worthwhile incorporating Sn in Ni/CeAl systems, a more in depth study needs to be undertaken. As such, a more detailed catalytic study has been conducted utilising different space velocities and reaction temperatures for both Ni-Sn/CeAl and Ni/CeAl, before a final set of stability tests were completed.

Fig. 8 presents the CH_4 and CO_2 conversion as well as the H_2/CO ratio as a function of time on stream, when the WHSV is varied from the standard 60,000 mL g^{-1} h^{-1} to 30,000 and 120,000 mL g^{-1} h^{-1}, at the same reaction temperature. What can be observed as a general rule from these plots is that as the WHSV increases, conversions decrease. For space velocities of 60,000 and 120,000 mL g^{-1} h^{-1}, both Ni/CeAl

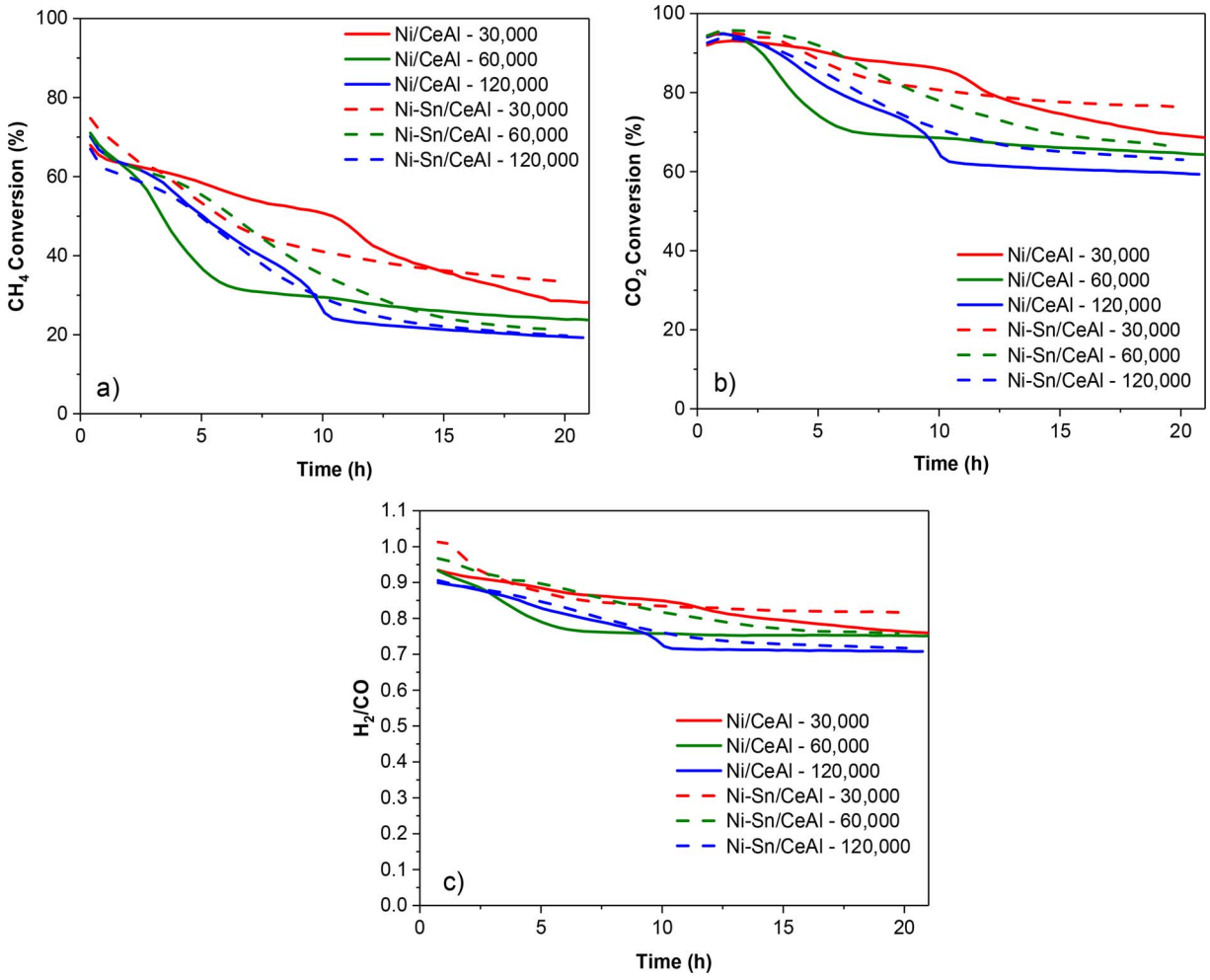

Fig. 8. WHSV experiments: a) CH_4 conversions (%), b) CO_2 conversions (%) and c) H_2/CO ratio (Reaction conditions: WHSV = 30,000–120,000 ml g^{-1} h^{-1}; CH_4:CO_2 = 1; P = 1 atm, T = 700 °C).

and Ni-Sn/CeAl stabilise at roughly the same value of 22% CH_4 conversion and 65% CO_2 conversion. At 60,000 mL g^{-1} h^{-1}, Ni/CeAl deactivates and stabilises first (after 5 hours) and Ni-Sn/CeAl deactivates and stabilises later (after 15 h). However, at 30,000 mL g^{-1} h^{-1} there is a marked difference in catalytic performance between the catalysts. Ni/CeAl begins to stabilise at the end of the experiment (20 h) with CH_4 and CO_2 conversions of roughly 30% and 70% respectively. The Ni-Sn/CeAl performs even better, starting to stabilise earlier (5 h) at higher CH_4 and CO_2 conversions of roughly 35% and 75% respectively. The later indicates the benefits of Sn as a promoter of Ni/CeAl catalysts, a promotional effect which seems be highlighted at lower space velocities. This is likely due to the longer residence times at lower space velocities, allowing more time for the gasification of carbon to occur, as such the poisoning by carbon is diminished. The general H_2/CO ratio trend for both catalysts is that, as the space velocity decreases from 120,000 mL g^{-1} h^{-1} to 30,000 mL g^{-1} h^{-1} the ratio increases from a minimum of 0.7 to a maximum of 0.825.

The effect of temperature on the catalytic performance of the prepared samples is shown in Fig. 9 in the form of H_2/CO ratios, coupled with CH_4 and CO_2 conversions as a function of time on stream. The general trend that can be observed is that as the temperature decreases from 800 to 600 °C, the conversions of CH_4 and CO_2 decrease dramatically. This has been well documented [8,10], and is attributed to the dry reforming reaction having highly endothermic characteristics, therefore requiring higher temperatures to progress at a faster rate. As explained previously, the catalysts run at 700 °C stabilise at roughly the same conversions for both CH_4 and CO_2 (25% and 65% respectively), with the Sn promoted catalyst having a higher conversion to begin with and stabilising later. The catalysts run at 600 °C, however, exhibit different results. It can be observed that Ni/CeAl stabilises almost instantly and holds steady. The conversions it stabilised at were also 25% and 65% CH_4 and CO_2 conversions respectively. However, for Ni-Sn/CeAl, a major drop in all conversions can be observed especially after 4 h, before stabilisation with conversions of virtual 0% and 35% for CH_4 and CO_2 respectively. For the catalysts run at 800 °C however, the conversion of CH_4 for both Ni/CeAl and Ni-Sn/CeAl exhibit deactivation before stabilising at 50% and 45% respectively. Also observable is the monometallic catalyst reaching a more stable steady state than the Sn promoted catalyst. By contrast, for the conversion of CO_2 it is clear that the Sn promoted catalyst suffers little deactivation, finishing at 85% conversion. Whereas for the base catalyst, deactivation occurs quickly (after 4 h), before stabilising at 75% conversion, reaching a more stable steady state. The suggested cause for this is the CeO_2 presence in both catalysts. In fact, CeO_2 promotes the reverse WGS reaction ($CO_2 + H_2 \rightleftharpoons CO + H_2O$) (even at high temperatures) which in turns may promote the SRM reactions ($CH_4 + H_2O \rightleftharpoons CO + 3H_2$; $CH_4 + 2H_2O \rightleftharpoons CO_2 + 4H_2$) meaning that more CH_4 is consumed increasing its conversion. At the same time, due to the SRM reaction being favoured, CO_2 is being produced as such there is a smaller respective conversion. The reason that the monometallic Ni/CeAl catalysts has a higher CH_4 but lower CO_2 conversion is due to its higher activity in the steam reforming reaction since more Ni is available for the reaction. In the bimetallic catalyst, Sn decorates the vicinity of Ni and although it improves Ni tolerance towards coking it may negatively

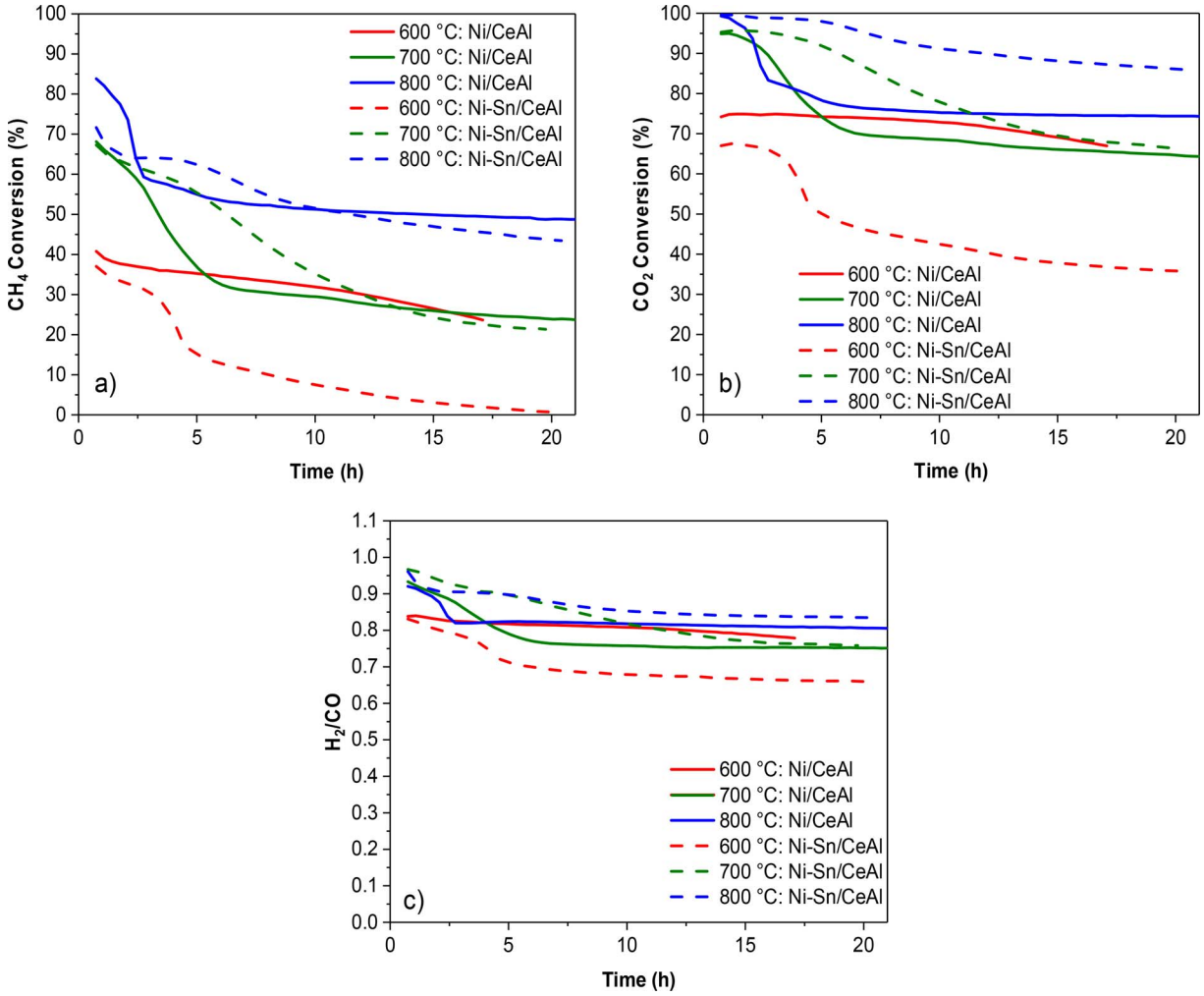

Fig. 9. Temperature experiments: a) CH_4 conversions (%), b) CO_2 conversions (%) and c) H_2/CO. (Reaction conditions: WHSV = 60,000 ml g^{-1} h^{-1}; CH_4:CO_2 = 1; P = 1 atm, T = 600–800 °C).

affect the activation of methane since there are less Ni active sites available. In summary, there is a trade-off between activity and stability; the presence of Sn helps to mitigate carbon deposition due to Sn's similar electronic structure to carbon, meaning Sn can occupy carbon nucleation positions, thus mitigating coking [30]. But it also may decrease the hydrocarbon reforming capacity of catalyst due to the active sites being smothered by Sn particles, preventing the reactants from accessing them, thereby reducing the activity. The pattern exhibited by the H_2/CO ratio is comparable to previous ratios, with the stabilised values ranging from 0.75 to 0.85. The exception to this is at 600 °C for the Sn promoted catalyst that presented a value of 0.65.

The long-term stability of the catalysts at 700 °C is displayed in Fig. 10, in which catalytic performance is plotted as a function of time on stream. The Sn promoted catalyst has higher activity to begin with and deactivates later than the base Ni/CeAl. However even though the base catalyst deactivates earlier, it stabilises at a higher conversion value for both CO_2 and CH_4. After the 90 + hour long experiment, the Ni-Sn/CeAl had conversions of 5% and 45% respectively whereas the Ni/CeAl had conversions of 15% and 55% respectively. This suggests that the monometallic catalyst is better in the long run, which is likely due to the catalyst having more active sites available. As a consequence of the catalytic activity results, the H_2/CO ratio follows a similar pattern as shown in the figure. In light of these results it seems that Sn prevents carbon deposition at early reaction stages (which is when typically carbon formation is more favoured) but for the long runs the fact that Sn could block some Ni active sites makes the monometallic approach a better choice. Certainly the optimisation of Sn loading could help to find the best compromise activity/stability.

4. Conclusions

Highly effective multicomponent Ni/CeO_2-Al_2O_3 catalysts for CO_2 conversion via dry reforming of methane have been developed in this study. Bimetallic combinations such as Ni-Pt and Ni-Sn have proven to exhibit different behaviour. In particular, Ni-Sn supported upon CeO_2-Al_2O_3 appeared to be a promising material, showing good H_2/CO ratios and high CO_2 conversions. This is due to the excellent redox properties of CeO_2, as well as the prevention of active phase sintering and subsequent carbon poisoning by the synergistic Sn-Ni interactions. However, the Ni-Pt system does not show a major advantage over the monometallic systems and therefore further studies exploring the optimum concentration of Pt promoter for Ni/CeAl in DRM would be desired.

Positive results with the Sn promoted catalyst where observed over varying WHSV and temperatures, outperforming the base Ni/CeAl catalyst in both. More specifically, when the conditions where changed to optimise the reaction (i.e. lower WHSV and higher temperature) the Sn promoted catalyst continued to outperform its Ni/CeAl counterpart.

The developed materials displayed high levels of CO_2 conversion during ca. 100 h continuous operation. Interestingly, for long-term runs the monometallic formulation performs better than the bimetallic Ni-Sn what indicates the influence of the active sites availability for

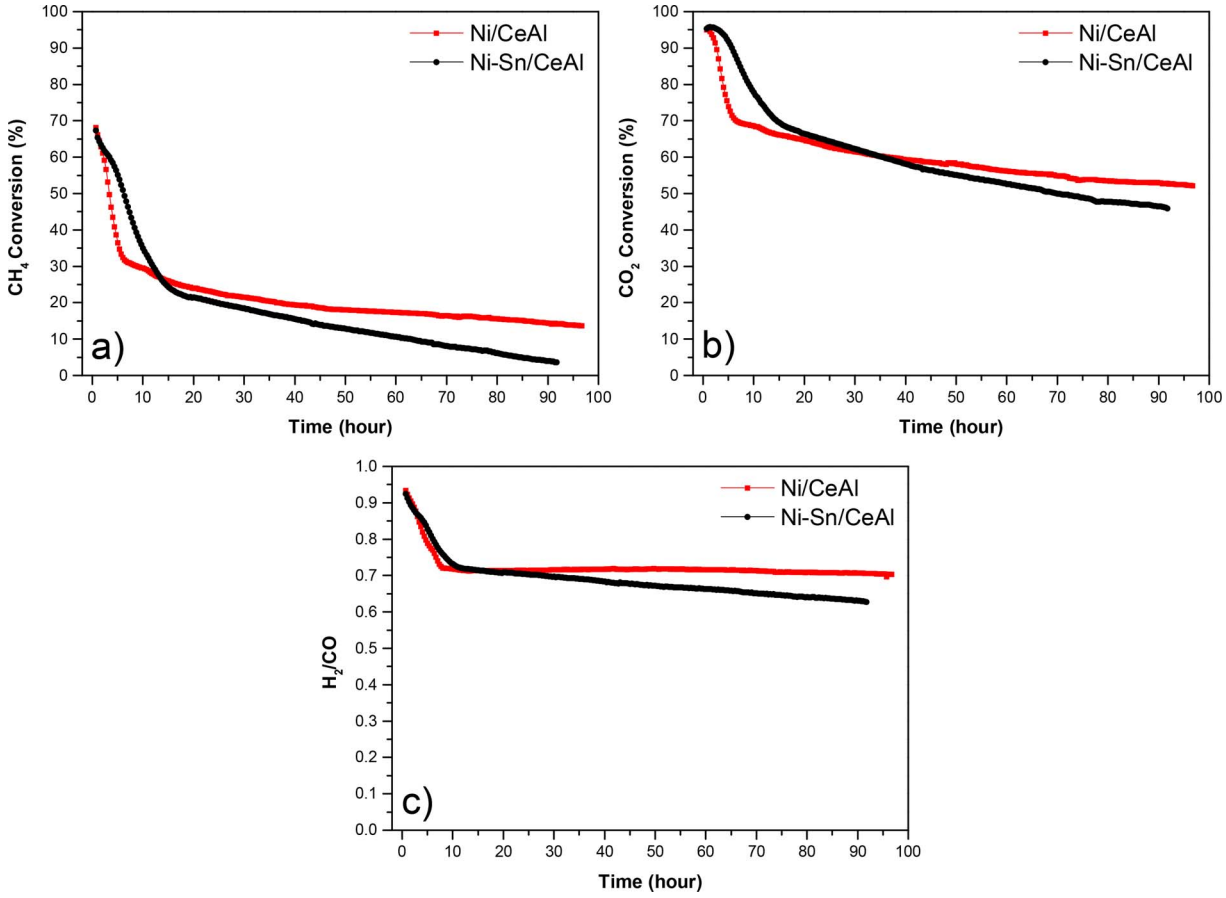

Fig. 10. Stability tests: a) CH_4 conversions (%), b) CO_2 conversions (%) and c) H_2/CO ratio (Reaction conditions: WHSV = 60,000 ml g^{-1} h^{-1}; CH_4:CO_2 = 1; P = 1 atm, T = 700 °C).

continuous runs. In any case our study provides useful guidelines in terms of catalysts formulation, effect of promoters and reaction conditions, to successfully develop highly active dry reforming materials with potential application in CO_2 utilisation technologies.

Acknowledgments

Financial support for this work was provided by the Department of Chemical and Process Engineering at the University of Surrey and the EPSRC under the projects EP/R512904/1 and EP/K036548/2. E. Le Saché acknowledges the Erasmus + programme for her fellowship which allowed her to conduct part of the experiments in Spain. The Spanish team acknowledges the financial support obtained from the Spanish Ministry of Economy and Competitiveness (ENE2015-66975-C3-2-R) and from Junta de Andalucía (TEP-8196), both co-financed by FEDER funds from the European Union. Sasol is kindly acknowledge for providing the alumina.

References

[1] J.G.J. Olivier, M. Muntean, J.A.H.W. Peters, Trends in Global CO2 Emissions: 2015 Report, (2015).
[2] K. Damen, M. Van Troost, A. Faaij, W. Turkenburg, A comparison of electricity and hydrogen production systems with CO2 capture and storage. Part A: review and selection of promising conversion and capture technologies, Prog. Energy Combust. Sci. 32 (2006) 215–246, http://dx.doi.org/10.1016/j.pecs.2005.11.005.
[3] T.C. Drage, K.M. Smith, C. Pevida, A. Arenillas, C.E. Snape, Development of adsorbent technologies for post-combustion CO2 capture, Energy Procedia. 1 (2009) 881–884, http://dx.doi.org/10.1016/j.egypro.2009.01.117.
[4] J.C.M. Pires, F.G. Martins, M.C.M. Alvim-Ferraz, M. Simoes, Recent developments on carbon capture and storage: an overview, Chem. Eng. Res. Des. 89 (2011) 1446–1460, http://dx.doi.org/10.1016/j.cherd.2011.01.028.
[5] D.Y.C. Leung, G. Caramanna, M.M. Maroto-Valer, An overview of current status of carbon dioxide capture and storage technologies, Renew. Sustain. Energy Rev. 39 (2014) 426–443, http://dx.doi.org/10.1016/j.rser.2014.07.093.
[6] N.D. Charisiou, A. Baklavaridis, V.G. Papadakis, M.A. Goula, Synthesis gas production via the biogas reforming reaction over Ni/MgO–Al2O3 and Ni/CaO–Al2O3 catalysts, Waste Biomass Valorization 7 (2016) 725–736, http://dx.doi.org/10.1007/s12649-016-9627-9.
[7] IPCC, Direct global warming potentials, IPCC fourth assess, Rep. Clim. Change 2007 (2007) 2.10.2.
[8] D. Pakhare, J. Spivey, A review of dry (CO_2) reforming of methane over noble metal catalysts, Chem. Soc. Rev. 43 (2014) 7813–7837, http://dx.doi.org/10.1039/C3CS60395D.
[9] G.C. de Araujo, S.M. de Lima, J.M. Assaf, M.A. Peña, J.L.G. Fierro, M. do, Carmo Rangel, Catalytic evaluation of perovskite-type oxide LaNi1-xRuxO3 in methane dry reforming, Catal. Today 133–135 (2008) 129–135, http://dx.doi.org/10.1016/j.cattod.2007.12.049.
[10] N.D. Charisiou, G. Siakavelas, K.N. Papageridis, A. Baklavaridis, L. Tzounis, D.G. Avraam, M.A. Goula, Syngas production via the biogas dry reforming reaction over nickel supported on modified with CeO2 and/or La2O3 alumina catalysts, J. Nat. Gas Sci. Eng. 31 (2016) 164–183, http://dx.doi.org/10.1016/j.jngse.2016.02.021.
[11] Y. Wang, L. Yao, S. Wang, D. Mao, C. Hu, Low-temperature catalytic CO2 dry reforming of methane on Ni-based catalysts: a review, Fuel Process. Technol. 169 (2018) 199–206, http://dx.doi.org/10.1016/J.FUPROC.2017.10.007.
[12] D.L. Trimm, Coke formation and minimisation during steam reforming reactions, Catal. Today 37 (1997) 233–238, http://dx.doi.org/10.1016/S0920-5861(97)00014-X.
[13] N. Kumar, M. Shojaee, J.J. Spivey, Catalytic bi-reforming of methane: from greenhouse gases to syngas, Curr. Opin. Chem. Eng. 9 (2015) 8–15, http://dx.doi.org/10.1016/j.coche.2015.07.003.
[14] G.A. Olah, A. Goeppert, M. Czaun, T. Mathew, R.B. May, G.K.S. Prakash, Single step Bi-reforming and oxidative Bi-reforming of methane (natural gas) with steam and carbon dioxide to metgas (CO-2H < inf > 2 < /inf >) for methanol synthesis: Self-sufficient effective and exclusive oxygenation of methane to methanol with oxygen, J. Am. Chem. Soc. 137 (2015) 8720–8729, http://dx.doi.org/10.1021/jacs.5b02029.
[15] S.S. Itkulova, G.D. Zakumbaeva, Y.Y. Nurmakanov, A.A. Mukazhanova, A.K. Yermaganbetova, Syngas production by bireforming of methane over Co-based alumina-supported catalysts, Catal. Today 228 (2014) 194–198, http://dx.doi.org/10.1016/j.cattod.2014.01.013.
[16] M.M. Danilova, Z.A. Fedorova, V.A. Kuzmin, V.I. Zaikovskii, A.V. Porsin, T. Krieger, Combined steam and carbon dioxide reforming of methane over porous nickel based catalysts, Catal. Sci. Technol. 5 (2015) 2761–2768, http://dx.doi.org/10.

1039/C4CY01614A.
[17] N. Rahemi, M. Haghighi, A.A. Babaluo, M.F. Jafari, P. Estifaee, Synthesis and physicochemical characterizations of Ni/Al2O3-ZrO2 nanocatalyst prepared via impregnation method and treated with non-thermal plasma for CO2 reforming of CH4, J. Ind. Eng. Chem. 19 (2013) 1566–1576, http://dx.doi.org/10.1016/j.jiec.2013.01.024.
[18] J. Guo, H. Lou, H. Zhao, D. Chai, X. Zheng, Dry reforming of methane over nickel catalysts supported on magnesium aluminate spinels, Appl. Catal. A Gen. 273 (2004) 75–82, http://dx.doi.org/10.1016/j.apcata.2004.06.014.
[19] Z. Hou, O. Yokota, T. Tanaka, T. Yashima, Surface properties of a coke-free Sn doped nickel catalyst for the CO2 reforming of methane, Appl. Surf. Sci. 233 (2004) 58–68, http://dx.doi.org/10.1016/j.apsusc.2004.03.223.
[20] Ş. Özkara-Aydnolu, A.E. Aksoylu, CO2 reforming of methane over Pt-Ni/Al2O3 catalysts: Effects of catalyst composition, and water and oxygen addition to the feed, Int. J. Hydrogen Energy 36 (2011) 2950–2959, http://dx.doi.org/10.1016/j.ijhydene.2010.11.080.
[21] Z. Hou, T. Yashima, Small amounts of Rh-promoted Ni catalysts for methane reforming with CO2, Catal. Lett. 89 (2003) 193–197, http://dx.doi.org/10.1023/A:1025746211314.
[22] W.K. Jóźwiak, M. Nowosielska, J. Rynkowski, Reforming of methane with carbon dioxide over supported bimetallic catalysts containing Ni and noble metal I. characterization and activity of SiO2 supported Ni-Rh catalysts, Appl. Catal. A Gen. 280 (2005) 233–244, http://dx.doi.org/10.1016/j.apcata.2004.11.003.
[23] Z. Hou, P. Chen, H. Fang, X. Zheng, T. Yashima, Production of synthesis gas via methane reforming with CO2 on noble metals and small amount of noble-(Rh-) promoted Ni catalysts, Int. J. Hydrogen Energy 31 (2006) 555–561, http://dx.doi.org/10.1016/j.ijhydene.2005.06.010.
[24] C. Crisafulli, S. Scire, R. Maggiore, S. Minico, S. Galvagno, CO_2 reforming of methane over Ni – Ru and Ni – Pd bimetallic catalysts, Catal. Lett. 59 (1999) 21–26.
[25] C. Crisafulli, S. Scirè, S. Minicò, L. Solarino, Ni – Ru bimetallic catalysts for the CO2 reforming of methane, Appl. Catal. 225 (2002) 1–9, http://dx.doi.org/10.1016/S0926-860X(01)00585-3.
[26] B. Pawelec, S. Damyanova, K. Arishtirova, J.L.G. Fierro, L. Petrov, Structural and surface features of PtNi catalysts for reforming of methane with CO2, Appl. Catal. A Gen. 323 (2007) 188–201, http://dx.doi.org/10.1016/j.apcata.2007.02.017.
[27] T.P. de Castro, E.B. Silveira, R.C. Rabelo-Neto, L.E.P. Borges, F.B. Noronha, Study of the performance of Pt/Al2O3 and Pt/CeO2/Al2O3 catalysts for steam reforming of toluene, methane and mixtures, Catal. Today 299 (2018) 251–262, http://dx.doi.org/10.1016/J.CATTOD.2017.05.067.
[28] L. Pastor-Pérez, A. Sepúlveda-Escribano, Multicomponent NiSnCeO2/C catalysts for the low-temperature glycerol steam reforming, Appl. Catal. A Gen. 529 (2017) 118–126, http://dx.doi.org/10.1016/j.apcata.2016.10.022.
[29] A. Löfberg, J. Guerrero-Caballero, T. Kane, A. Rubbens, L. Jalowiecki-Duhamel, Ni/CeO2 based catalysts as oxygen vectors for the chemical looping dry reforming of methane for syngas production, Appl. Catal. B Environ. 212 (2017) 159–174, http://dx.doi.org/10.1016/J.APCATB.2017.04.048.
[30] T. Stroud, T.J. Smith, E. Le Saché, J.L. Santos, M.A. Centeno, H. Arellano-Garcia, J.A. Odriozola, T.R. Reina, Chemical CO 2 recycling via dry and bi reforming of methane using Ni-Sn/Al 2 O 3 and Ni-Sn/CeO 2 -Al 2 O 3 catalysts, Appl. Catal. B Environ. 224 (2018) 125–135, http://dx.doi.org/10.1016/j.apcatb.2017.10.047.
[31] M. García-Diéguez, I.S. Pieta, M.C. Herrera, M.A. Larrubia, L.J. Alemany, Nanostructured Pt- and Ni-based catalysts for CO2-reforming of methane, J. Catal. 270 (2010) 136–145, http://dx.doi.org/10.1016/J.JCAT.2009.12.010.
[32] X. Yu, F. Zhang, N. Wang, S. Hao, W. Chu, Plasma-treated bimetallic Ni–Pt catalysts derived from hydrotalcites for the carbon dioxide reforming of methane, Catal. Lett. 144 (2014) 293–300, http://dx.doi.org/10.1007/s10562-013-1130-3.
[33] E. Nikolla, J. Schwank, S. Linic, Promotion of the long-term stability of reforming Ni catalysts by surface alloying, J. Catal. 250 (2007) 85–93, http://dx.doi.org/10.1016/J.JCAT.2007.04.020.
[34] H. Wu, V. La Parola, G. Pantaleo, F. Puleo, M.A. Venezia, F.L. Liotta, Ni-based catalysts for low temperature methane steam reforming: recent results on Ni-Au and comparison with other Bi-metallic systems, Catalysts 3 (2013), http://dx.doi.org/10.3390/catal3020563.
[35] A. Penkova, L. Bobadilla, S. Ivanova, M.I. Domínguez, F. Romero-Sarria, A.C. Roger, M.A. Centeno, J.A. Odriozola, Hydrogen production by methanol steam reforming on NiSn/MgO–Al2O3 catalysts: the role of MgO addition, Appl. Catal. A Gen. 392 (2011) 184–191, http://dx.doi.org/10.1016/j.apcata.2010.11.016.
[36] A.S. Prakash, C. Shivakumara, M.S. Hegde, Single step preparation of CeO2/CeAlO3/γ-Al2O3 by solution combustion method: phase evolution, thermal stability and surface modification, Mater. Sci. Eng. B Solid-State Mater. Adv. Technol. 139 (2007) 55–61, http://dx.doi.org/10.1016/j.mseb.2007.01.034.
[37] J.Z. Shyu, K. Otto, Characterization of Pt/γ-alumina catalysts containing ceria, J. Catal. 115 (1989) 16–23, http://dx.doi.org/10.1016/0021-9517(89)90003-1.
[38] N.K. Nga, D.K. Chi, Synthesis, characterization and catalytic activity of CoAl2O4 and NiAl2O4 spinel - type oxides for NOx selective reduction, Adv. Technol. Mater. Mater. Process. 6 (2004) 336–343, http://dx.doi.org/10.2240/azojomo0129.
[39] H. Liu, P. Da Costa, H.B. Hadj Taief, M. Benzina, M.E. Gálvez, Ceria and zirconia modified natural clay based nickel catalysts for dry reforming of methane, Int. J. Hydrogen Energy 42 (2017) 23508–23516, http://dx.doi.org/10.1016/J.IJHYDENE.2017.01.075.
[40] H.-S. Roh, H.S. Potdar, K.-W. Jun, J.-W. Kim, Y.-S. Oh, Carbon dioxide reforming of methane over Ni incorporated into Ce–ZrO2 catalysts, Appl. Catal. A Gen. 276 (2004) 231–239, http://dx.doi.org/10.1016/j.apcata.2004.08.009.
[41] M.A. Goula, N.D. Charisiou, K.N. Papageridis, A. Delimitis, E. Pachatouridou, E.F. Iliopoulou, Nickel on alumina catalysts for the production of hydrogen rich mixtures via the biogas dry reforming reaction: Influence of the synthesis method, Int. J. Hydrogen Energy 40 (2015) 9183–9200, http://dx.doi.org/10.1016/J.IJHYDENE.2015.05.129.
[42] S.R. de Miguel, I.M.J. Vilella, S.P. Maina, D. San José-Alonso, M.C. Román-Martínez, M.J. Illán-Gómez, Influence of Pt addition to Ni catalysts on the catalytic performance for long term dry reforming of methane, Appl. Catal. A Gen. 435–436 (2012) 10–18, http://dx.doi.org/10.1016/J.APCATA.2012.05.030.
[43] S. Wang, G.Q. Lu, Role of CeO2 in Ni/CeO2-Al2O3 catalysts for carbon dioxide reforming of methane, Appl. Catal. B Environ. 19 (1998) 267–277, http://dx.doi.org/10.1016/S0926-3373(98)00081-2.
[44] J.H. Vleeming, B.F.M. Kuster, G.B. Marin, Effect of platinum particle size and catalyst support on the platinum catalyzed selective oxidation of carbohydrates, Catal. Letters. 46 (1997) 187–194.
[45] S. Sepehri, M. Rezaei, Ce promoting effect on the activity and coke formation of Ni catalysts supported on mesoporous nanocrystalline γ-Al2O3 in autothermal reforming of methane, Int. J. Hydrogen Energy 42 (2017) 11130–11138, http://dx.doi.org/10.1016/J.IJHYDENE.2017.01.096.
[46] M.A. Muñoz, J.J. Calvino, J.M. Rodríguez-Izquierdo, G. Blanco, D.C. Arias, J.A. Pérez-Omil, J.C. Hernández-Garrido, J.M. González-Leal, M.A. Cauqui, M.P. Yeste, Highly stable ceria-zirconia-yttria supported Ni catalysts for syngas production by CO2 reforming of methane, Appl. Surf. Sci. 426 (2017) 864–873, http://dx.doi.org/10.1016/J.APSUSC.2017.07.210.
[47] A.C. Ferrari, J. Robertson, Interpretation of Raman spectra of disordered and amorphous carbon, Phys. Rev. B. 61 (2000) 14095–14107, http://dx.doi.org/10.1103/PhysRevB.61.14095.
[48] S. Piscanec, F. Mauri, A.C. Ferrari, M. Lazzeri, Ab initio resonant Raman spectra of diamond-like carbons, Diam. Relat. Mater. 14 (2005) 1078–1083, http://dx.doi.org/10.1016/J.DIAMOND.2004.11.043.
[49] R. Dębek, M. Radlik, M. Motak, M.E. Galvez, W. Turek, P. Da Costa, T. Grzybek, Ni-containing Ce-promoted hydrotalcite derived materials as catalysts for methane reforming with carbon dioxide at low temperature – on the effect of basicity, Catal. Today 257 (2015) 59–65, http://dx.doi.org/10.1016/j.cattod.2015.03.017.
[50] R. Dębek, M. Motak, M.E. Galvez, T. Grzybek, P. Da Costa, Influence of Ce/Zr molar ratio on catalytic performance of hydrotalcite-derived catalysts at low temperature CO2 methane reforming, Int. J. Hydrogen Energy 42 (2017) 23556–23567, http://dx.doi.org/10.1016/J.IJHYDENE.2016.12.121.
[51] P. Chen, H.-B. Zhang, G.-D. Lin, K.-R. Tsai, Development of coking-resistant Ni-based catalyst for partial oxidation and CO2-reforming of methane to syngas, Appl. Catal. A Gen. 166 (1998) 343–350, http://dx.doi.org/10.1016/S0926-860X(97)00291-3.